Paper No.
79-DET-56

an ASME publication

$3.00 PER COPY $1.50 TO ASME MEMBERS

J. C. NICHOLAS

Analytical Engineer,
Turbo Engineering Sciences,
Ingersoll-Rand Co.,
Phillipsburg, N. J. 08865

L. E. BARRETT

Research Asst. Professor,
Department of Mechanical and
Aerospace Engineering,
University of Virginia,
Charlottesville, Va. 22901

M. E. LEADER

Engineer,
Monsanto Chemical Intermediates Co.,
Texas City, Tex. 77568

Experimental-Theoretical Comparison of Instability Onset Speeds for a Three Mass Rotor Supported by Step Journal Bearings

Theoretically predicted instability onset speeds are compared to the experimental instability threshold speeds for a simple three mass flexible rotor supported by five geometrically different sets of step journal bearings and a set of two axial groove bearings. The near optimum step bearing designs increase the instability onset speed by around 109 percent in one case and 41 percent in another compared to two ax,al groove bearings. The off optimum designs increase the instability speed by 18, 30 and 35 percent. The theoretical stability analysis predicts the general trends in the experimental data.

Introduction

The step journal or pressure dam bearing has been one of the American rotating equipment industry's standard bearings for many years. Some examples include turbine manufacturers who equip many of their machines with step bearings prior to sale. Pressure dam bearings are extremely popular in the petro-clemical industry where a large percentage of the industry's turbomachinery operates on these bearings.

Other applications include high speed gear boxes where the gear loading may vary from several thousand to only a few hundred pounds. This large variance in load is often accompanied by a change in load direction. An example is the gear box between a motor/generator and a drive turbine on a compressor train. In this type of application, step bearings are used to insure stable operation when the gear loading is small.

Some of the relevant references contained in the literature concerning pressure dam bearing design and application are listed here [1–10]. The relative importance of inertia effects at the step and turbulence in the pocket is dicussed in references [5, 6]. Step design for maximum load capacity is considered in references [1–3, 6]. Optimum step bearing designs for favorable rotor-bearing stability are suggested in references [7–9]. Reference [8] also contains the dynamic stiffness and damping properties for different step bearing geometries.

Experimental results for different step configurations may be found in references [4, 5, 9, 10]. A theoztical-experimental comparison of the instability onset speed for a three mass flexible rotor is presented in reference [8]. The rotor is supported by three different sets of bearings: two axial groove bearings, a poor step bearing design and a near optimum step bearing design.

This work is an extension of the theoretical-experimental comparison of [8]. Five different step bearing geometries and a two axial groove bearing are considered. The pressure dam bearings employed have different step heights and locations. Optimum and off-optimum designs are used. Instability onset speeds are determined both theoretically and experimentally and a comparison is made to determine the accuracy of the theoretical analysis.

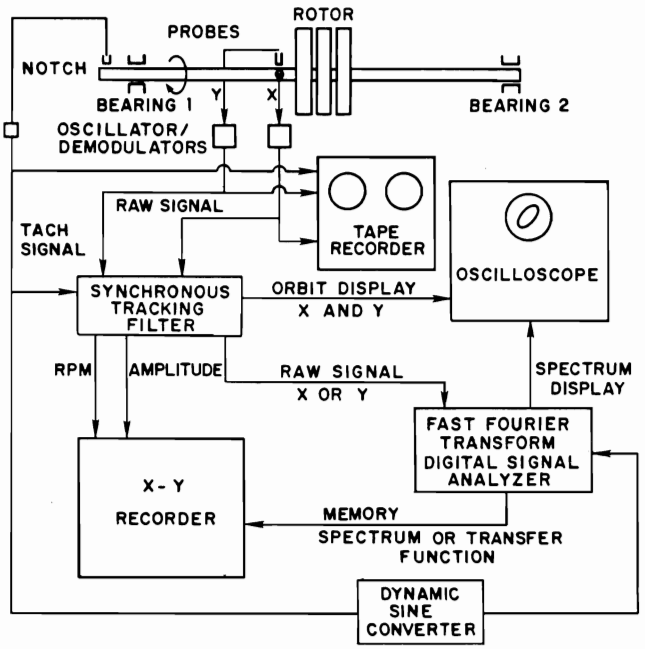

Fig. 1 Instrumentation schematic

Rotor and Bearing Geometries

A three mass flexible rotor mounted symmetrically between two bearing supports was used to obtain the experimental results.

Contributed by the Vibrations Committee for presentation at the Design Engineering Technical Conference, St. Louis, Mo., Sept. 10–12, 1979 of the AMERICAN SOCIETY OF MECHANICAL ENGINEERS. Manuscript received at ASME Headquarters June 7, 1979. Paper No. 79-DET-56.

Copies will be available until Sept. 1980.

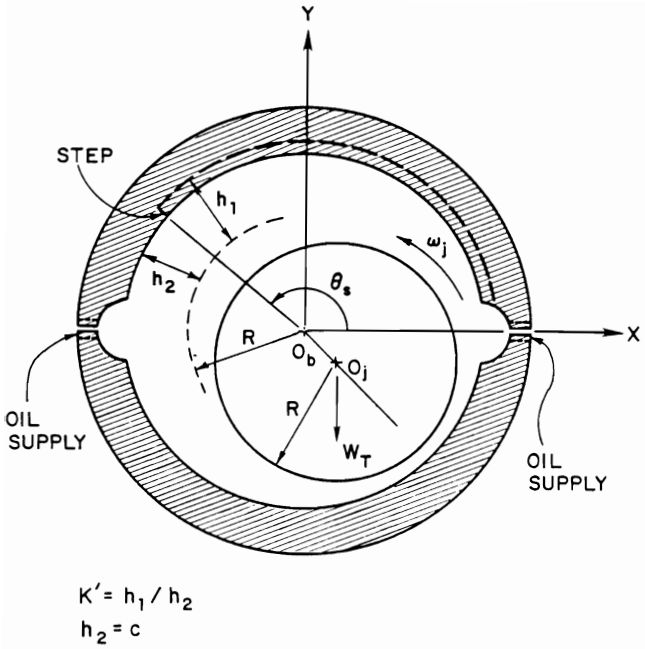

Fig. 2 Step bearing schematic, end view

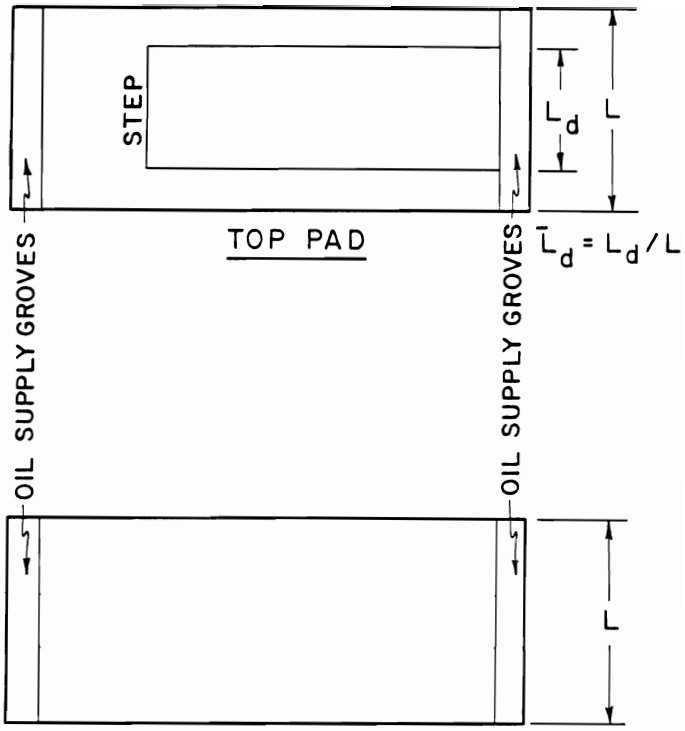

Fig. 3 Step bearing schematic, top and bottom pads

The rotor's mass is lumped in the center as shown in Fig. 1. The total rotor weight is 132.6 N (29.8 lbs), the bearing span is 53.34 cm (21.0 in) and the shaft diameter (cold) at the bearing supports is 2.540 cm (1.000 in). The rotor is driven by a one horsepower DC motor. The oil supply temperature is variable, but was maintained at 54°C during the tests.

A noncontacting probe mounted near the shaft center was used to monitor the horizontal shaft vibration (Fig. 1). Fig. 1 also includes a schematic of the instrumentation. Additional details of the experimental procedure may be found in references (9, 10].

All six pairs of bearings considered have two axial oil supply grooves located at the horizontal split (Fig. 2). These grooves are 20 degrees in arc length making the arc length of both top and bottom pads 160 degrees. The step and two axial groove bearings do not contain a circumferential relief groove in the bottom pad. The two axial groove bearings are identical to the pressure dam design with $h_1 = h_2$ in Fig. 2. The length to diameter ratio for each bearing is 1.0 with $D = 2.54$ cm.

Ideally, each bearing was to have a 5.08×10^{-3} cm (2.0 mil) radial clearance. However, due to difficulties in manufacturing, the radial clearance ranged from 4.57×10^{-3} cm (1.8 to 2.5 mils). The clearance was measured cold with a dial micrometer. Several readings were taken and the average value used.

The important geometric parameters in step bearing design are the film thickness ratio, K', and the dam location, θ_s [7]. The ratio of film thicknesses is defined as h_1/h_2 when the shaft is centered in the bearing (Fig. 2). Thus

$$K' = h_1/h_2$$

$$K' = h_1/c$$

where h_1 = centered clearance inside pocket

The dam location angle, θ_s, is measured with rotation from the

Nomenclature

c, c_1, c_2 = bearing radial clearance, number one bearing, number two bearing (L)
$C_{xx}, C_{xy}, C_{yx}, C_{yy}$ = bearing damping coefficients (FTL^{-1})
$\bar{C}_{xx}, \bar{C}_{xy}, \bar{C}_{yx}, \bar{C}_{yy}$ = dimensionless damping coefficients, $\bar{C}_{xx} = C_{xx}(\omega_j c/W_T)$
D = shaft diameter (L)
e_b = bearing eccentricity (L)
g = gravitational constant (LT^{-2})
h_1, h_2 = film thickness before, after step, centered bearing ($h_2 = c$) (L)
$K_{xx}, K_{xy}, K_{yx}, K_{yy}$ = bearing stiffness coefficients (FL^{-1})
$\bar{K}_{xx}, \bar{K}_{xy}, \bar{K}_{yx}, \bar{K}_{yy}$ = dimensionless stiffness coefficients, $\bar{K}_{xx} = K_{xx}(c/W_T)$
$K' = \frac{h_1}{h_2} = \frac{h_1}{c}$, film thickness ratio
L = bearing axial length (L)
L_s = rotor bearing span [L]
L_d, L_t = step bearing axial dam length, relief track axial length (L)
$\bar{L}_d, \bar{L}_t$ = $L_d/L, L_t/L$, step bearing axial dam length ratio, relief track axial length ratio
N, N_s = shaft rotational speed (rpm), (rps)
O_b, O_j = bearing, journal center
R = radius of shaft (journal) (L)
$S = \frac{\mu N_s L D}{W_T}\left(\frac{R}{c}\right)^2$, Sommerfeld number
W_T = bearing external load (F)
W_s = rotor total weight (F)
X, Y = coordinate system for rotating journal in bearing housing
X_2 = horizontal probe location
ϵ_b = e_b/c, bearing eccentricity ratio
θ_s = location of step measured with rotation from positive X-axis (degrees)
μ = average fluid viscosity (FTL^{-2})
χ = pad arc length (degrees)
ω_j = shaft rotational speed (T^{-1})
ω_s = $\omega_j \sqrt{c/g}$, threshold speed, horizontal rotor

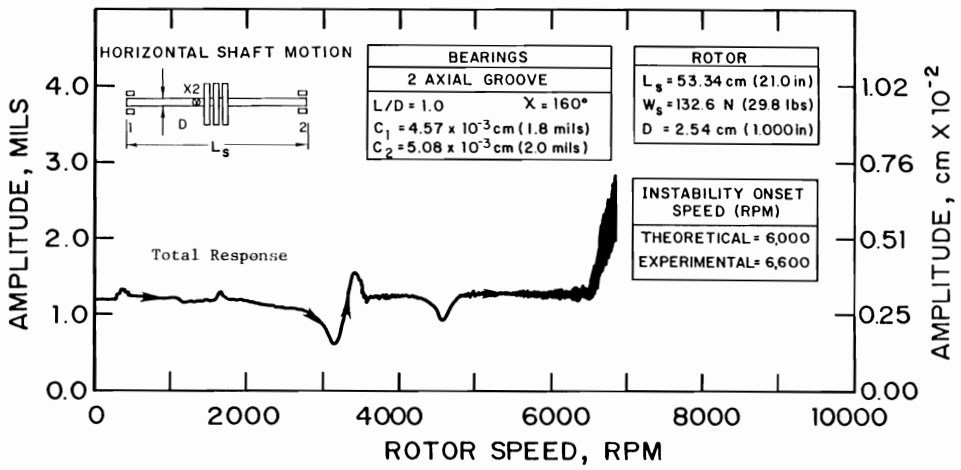

Fig. 4 Total response, two axial groove bearings

Table 1 Summary of geometric parameters for the six bearing sets. Dual numbers for each set refer to left and right end bearings.

Bearing Set No.	Type	K'	θ_s	c (cm x 10^3)	c (mils)	Dam Height = h - c (cm x 10^{-1})	Dam Height = h - c (mils)	$\bar{L}_d$
A	Two Axial Groove	1.0 1.0	- -	4.57 5.08	1.8 2.0	0.0 0.0	0.0 0.0	- -
1	Step	2.1 2.4	145°	5.59 6.35	2.2 2.5	6.10 8.89	2.4 3.5	0.75
2	Step	2.8 2.6	140°	6.35 6.35	2.5 2.5	11.43 10.16	4.5 4.0	0.75
3*	Step	6.6 * 8.6	150°	6.10 6.35	2.4 2.5	34.04 48.26	13.04 19.0	0.75
4*	Step	3.3 2.1	90°*	6.10 6.10	2.4 2.4	13.97 6.60	5.5 2.6	0.75
5*	Step	11.7 * 8.3	140°	5.33 6.10	2.1 2.4	57.15 44.45	22.5 17.5	0.50

Common to all bearings: L/D = 1.0, $\bar{L}_t$ = 0.0, χ = 160°
*Off-optimum

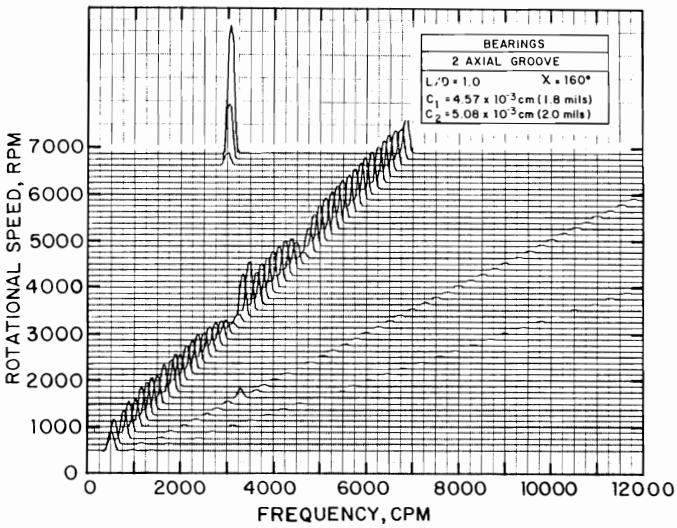

Fig. 5 Frequency spectrum, two axial groove bearings

positive X (horizontal) axis. Optimum values for favorable stability are around $K' = 3.0$ and $\theta_s = 125°$ to $150°$ [7]. Other parameters are the dam axial length ratio $\bar{L}_d = \bar{L}_d/L$ (Fig. 3) and the relief groove axial length ratio $\bar{L}_t = L_t/L$. For all cases, $L_t = 0.0$ since the bottom pad does not have a circumferential relief groove.

A summary of these parameters are listed in Table 1 for all six sets of bearings. Note that step bearing sets 1 and 2 represent the near optimum design [8] with film thickness ratios between 2.1 and 2.8. Sets 3 and 5 are off-optimum designs with larger K' values between 6.6 and 11.7. The off-optimum angular location is represented by set 4 with $\theta_s = 90°$. The dual numbers in the tables refer to the left (motor) and right ends of the test rotor respectively.

Experimental Results

To obtain the experimental instability onset speed, the rotor is accelerated until a large subsynchronous vibration component is observed. Speed-amplitude plots are shown here for the six different bearing sets. For three cases, frequency spectrums are also included.

Fig. 4 illustrates the total rotor response with two axial groove bearings. Fig. 5 is a frequency spectrum for the same case. The subsynchronous component first appears at about $N = 6{,}600$ rpm.

The total response for a near optimum step bearing design (set number 1) is shown in Fig. 6 with a corresponding frequency spectrum in Fig. 7. This design features a step at $\theta_s = 145°$ and film thickness ratios of 2.1 and 2.4. The rotor was run up to maximum speed without a large subsynchronous component appearing. However, two small peaks appear in Fig. 6 at around 10,500 rpm and 12,000 rpm. Fig. 7 shows a slight nonsynchronous "bump" at 12,000 rpm (frequency around 3300 rpm). It appears that the rotor may be on the instability threshold at 12,000 rpm.

Fig. 8 is a speed-amplitude plot for another, nearly identical optimum design (set number 2) with $\theta_s = 140°$ and $K' = 2.8$, 2.6. For this case, the onset of instability is around $N = 9{,}300$ rpm.

An off optimum design (set number 3) is shown in Fig. 9 (speed-amplitude) and 10 (frequency spectrum). This design retains the near optimum $\theta_s = 150°$ but the film thickness ratios are larger with $K' = 6.6$ and 8.6. A large subsynchronous vibration component appears at approximately $N = 8{,}900$ rpm.

Pressure dam set number 4 has near optimum film thickness ratios of 3.3 and 2.1. However, the step is located at $\theta_s = 90°$. Fig. 11 shows that the instability occurs at around $N = 8{,}600$ rpm.

The final case is another off optimum design with $\theta_s = 140°$ and $K' = 11.7$ and 8.3. It should also be noted that the dam axial length ratio is $\bar{L}_d = 0.5$ while the other step bearing designs have a dam length ratio of 0.75 (Table 1). Fig. 12 indicates the onset of instability occurs at N = 7,800 rpm.

Table 2 summarizes the experimental results. The near optimum designs (sets 1 and 2) increase the instability onset speed by 109 and 41 percent respectively over the two axial groove bearings. The off optimum designs (sets 3, 4 and 5) increase the instability speed by 35, 30 and 18 percent respectively.

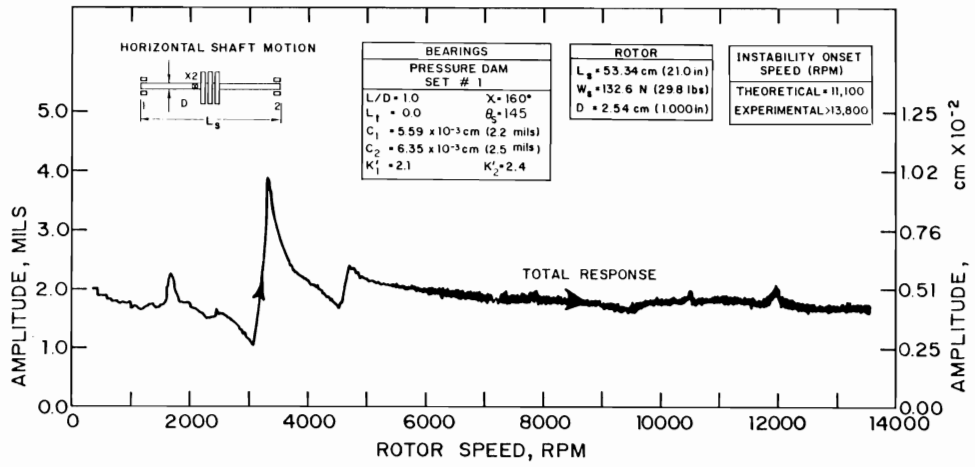

Fig. 6 Total response, step bearing set number 1, near optimum design

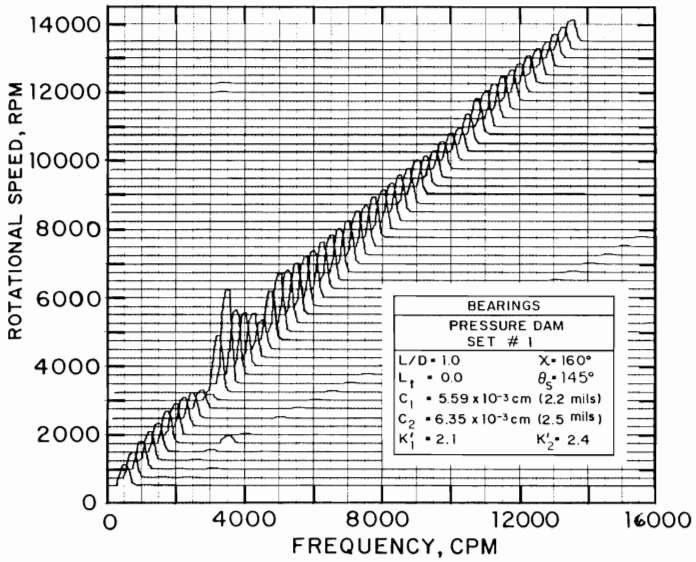

Fig. 7 Frequency spectrum, step bearing set number 1, near optimum designs

Comparing step bearing set number 3 to number 5, increasing the film thickness ratios from 6.6 and 8.6 to 11.7 and 8.3 decreases the instability speed by 12 percent. This trend is somewhat tainted since the dam axial length ratio is smaller for set 5 compared to set 3. Also, the step locations differ by 10°.

Theoretical Results

To obtain the theoretical instability onset speeds, the stiffness and damping properties of the bearings must be determined. The dynamic properties for all six sets of bearings were calculated using a finite length step bearing computer program that solves Reynolds equation using finite elements [11]. The same program generated the step bearing characteristic curves in reference [8]. The speed dependent characteristics are used as input data to a stability program that employs a transfer matrix approach similar to the method presented in reference [12].

The rotor model used in the stability computer program is given in Table 3. The dynamic properties of a sample bearing (set number 1) are summarized as a function of rotor speed in Tables 4 (stiffness properties) and 5 (damping properties).

Table 6 compares the Sommerfeld number, eccentricity ratio and rigid rotor stability parameter, ω_s [7] for all six bearing sets at 8000 rpm. The Sommerfeld number for all bearings is greater than 2.0, which is the optimum range for step bearings designed to improve stability [7]. The two axial groove bearings operate at an eccentricity ratio of around 0.035. The step bearings, due to the step loading, operate between $\epsilon = 0.29$ for a near optimum design (set number 1) and 0.09 for an off optimum design (set number 5). The rigid rotor stability parameter indicates that all five step bearing designs have larger ω_s values compared to the off optimum designs. Insight into the relative effectiveness of the step may be gained by comparing ϵ and ω_s for the 5 sets of pressure dam bearings. Set number 5 has the largest film thickness ratios, the smallest eccentricity ratios and the smallest ω_s values compared to the other step bearings. It is therefore anticipated that set number 5 should have the lowest instability onset speed for the step bearing designs.

The theoretical instability onset speed is determined by examining the real part of the eigenvalue. As an example, Table 7 lists the real part of the eigenvalues as a function of rotor speed for step bearing set number 1. The onset of instability theoretically occurs when the real root equals zero.

Table 8 summarizes the results of the theoretical stability analysis. The experimental results are also indicated along with the percent error in the theoretical predictions. The error is under 10 percent for all cases except bearing sets 1 and 2. Set number 1 has an error greater than 19.6 percent. Set number 2 over estimates the onset speed by 23.7 percent. All other cases theoretically under predict the instability speed.

Discussion of Results

The theoretical stability analysis predicts the general trends in the experimental data. All step gearing designs increase the onset speed over the two axial groove case. Comparing all step bearing cases, the near-optimum designs have the highest onset speeds and the off-optimum designs the lowest.

The analysis for step bearing set number 1 shows an error greater than 19.6 percent. The theoretical onset speed is 11,100 rpm. However, set number 1 shows two small peaks around 10,500 and 12,000 rpm (Fig. 6) and a very small 3300 CPM component at about 12,000 rpm (Fig. 7).

Set number 2 over estimates the onset speed by 23.7 percent. Closer examination of step bearing set 2 shows that the pockets on both bearings are not of uniform depth. This is not the case for the other step bearing sets. Near the step, the pocket depth for set 2 is 11.2×10^{-3} (4.4 mils) and 10.4×10^{-3} cm (4.1 mils). This results in the film thickness ratios indicated in the tables and used in the analysis ($K' = 2.8, 2.6$). Upstream of the step, the pocket depth decreases to around 2.5×10^{-3} cm (1.0 mils) for both bearings.

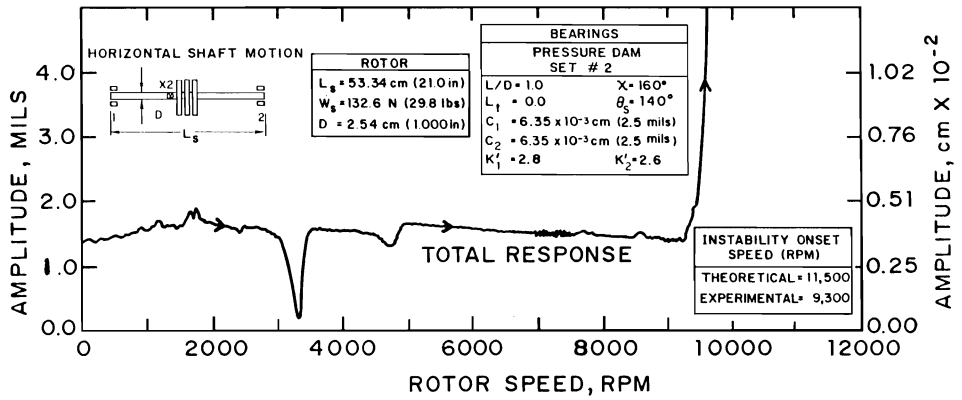

Fig. 8 Total response, step bearing set number 2, near optimum design

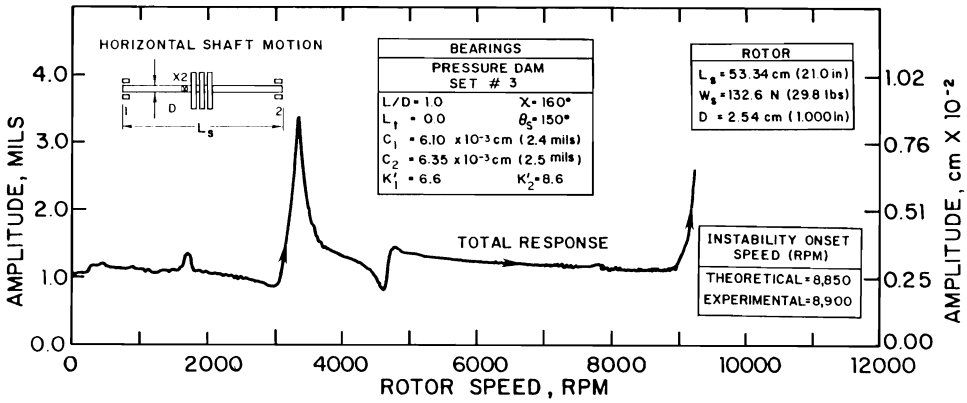

Fig. 9 Total response, step bearing set number 3, off-optimum film thickness ratios

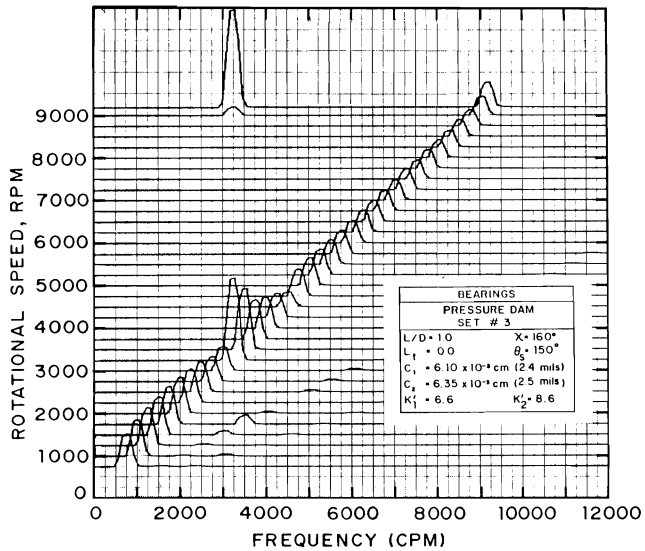

Fig. 10 Frequency spectrum, step bearing set number 3, off-optimum film thickness ratio

Table 2 Summary of experimental instability onset speeds for the six bearing cases

Bearing Set No.	Type	K'	θ_s	Experimental Onset Speed (RPM)
A	Two Axial Groove	1.0	-	6,600
1	Step	2.1,2.4	145°	>13,800
2	Step	2.8,2.6	140°	9,300
3*	Step	6.6,8.6*	150°	8,900
4*	Step	3.3,2.1	90°*	8,600
5*	Step	11.7,8.3*	140°	7,800

* Off-optimum

The side rails are known to be important in determining the stability characteristics provided by step bearings [4]. If the side rails are not deep enough (ideally, as deep as the step), the pressure build-up inside the pocket is diminshed and the effect of the step is reduced. The approximate this effect theoretically, the analysis was repeated with a film thickness ratio of 1.5 for both bearings. The predicted onset speed is reduced to 8,200 rpm.

The biggest problem with the analysis is that the bearings are of small dimensions. Requested tolerances on the clearance, dam height, step location and pocket depth were difficult to hold. Measurement of these quantities was also a problem. The small size also produced a Reynolds number based on a radial clearance of 5.08×10^{-3} (2.0 mils) of 8.94 at 8000 rpm. Thus, the load produced by the step is predominantly due to viscous effects and not turbulence in the pocket.

Conclusions

The near optimum pressure dam bearing designs increase the

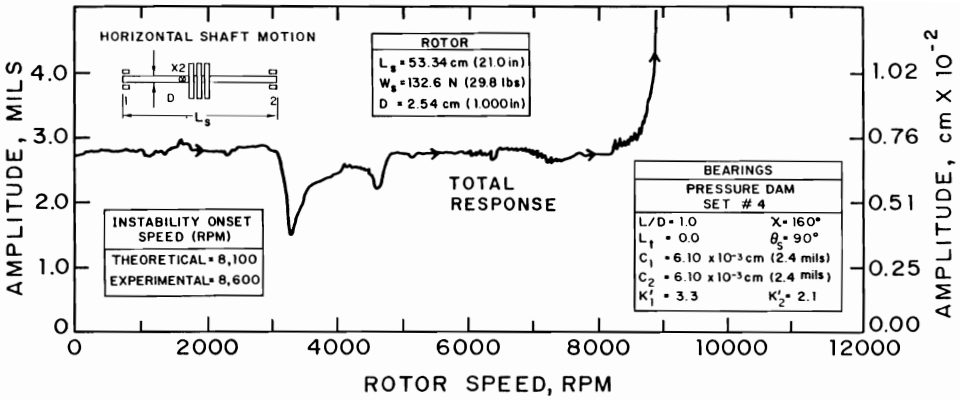

Fig. 11 Total response, step bearing set number 4, off-optimum step location

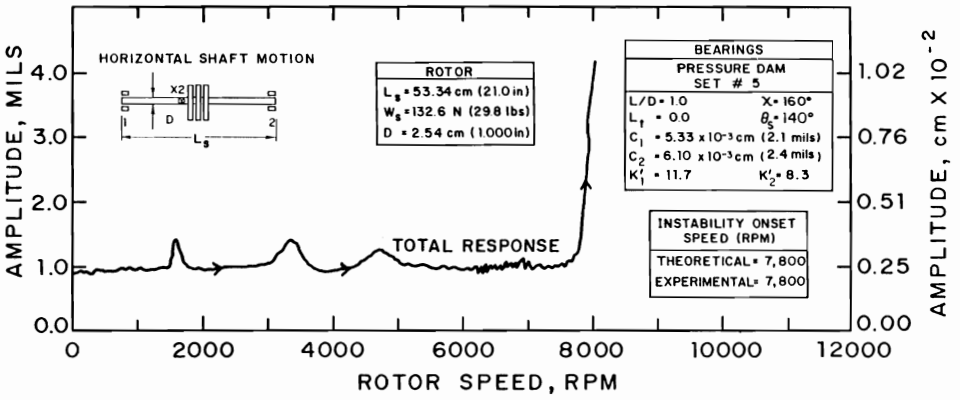

Fig. 12 Total response, step bearing set number 5, off-optimum film thickness ratio

Table 3 Rotor model used in the stability computer program

Station Number	Station Length		Outside Diameter				External*** Weight	
			Stiffness		Weight**			
	in	cm	in	cm	in	cm	lbs	N
1	3.20	8.13	1.00	2.54				
2*	1.00	2.54	1.00	2.54				
3	2.30	5.84	1.00	2.54				
4	1.50	3.81	1.00	2.54				
5	1.50	3.81	1.00	2.54				
6	2.25	5.72	1.00	2.54				
7	0.52	1.32	1.00	2.54				
8	0.31	0.79	1.00	2.54				
9	1.00	2.54	6.00	15.24	1.00	2.54	3.95	17.57
10	0.36	0.91	1.00	2.54			3.95	17.57
11	1.00	2.54	6.00	15.24	1.00	2.54	3.95	17.57
12	0.36	0.91	1.00	2.54			3.95	17.57
13	1.00	2.54	6.00	15.24	1.00	2.54	3.95	17.57
14	0.45	1.14	1.00	2.54			3.95	17.57
15	2.25	5.72	1.00	2.54				
16	1.50	3.81	1.00	2.54				
17	1.50	3.81	1.00	2.54				
18	1.75	4.44	1.00	2.54				
19	0.25	0.64	1.63	4.14				
20	0.30	0.76	1.00	2.54				
21*	1.00	2.54	1.00	2.54				
22	0.20	0.51	1.00	2.54				
23	0.45	1.14	1.63	4.14				
24	0.00	0.00	1.63	4.14				

* Bearing locations
** Blanks in outside weight diameter column indicate same values as stiffness diameter
*** Blanks in external weight column indicate zero

Table 4 Stiffness properties - step bearing set number 1

	Speed RPM	$K_{xx} \times 10^{-4}$		$K_{xy} \times 10^{-4}$		$K_{yx} \times 10^{-5}$		$K_{yy} \times 10^{-4}$	
		lbs/in	N/cm	lbs/in	N/cm	lbs/in	N/cm	lbs/in	N/cm
Number 1 Bearing	8,000	6.82	11.94	1.64	2.87	-2.43	-4.26	6.68	11.70
	10,000	8.46	14.81	1.96	3.43	-2.97	-5.20	8.32	14.57
	12,000	10.11	17.70	2.29	4.01	-3.57	-6.25	9.96	17.44
	14,000	11.77	20.61	2.61	4.57	-4.17	-7.30	11.61	20.33
	16,000	13.44	23.54	2.94	5.15	-4.77	-8.35	13.26	23.22
Number 2 Bearing	8,000	5.24	9.18	1.00	1.75	-1.56	-2.73	5.44	9.53
	10,000	6.46	11.31	1.16	2.03	-1.95	-3.41	6.74	11.80
	12,000	7.69	13.47	1.32	2.31	-2.33	-4.08	8.04	14.08
	14,000	8.93	15.64	1.47	2.57	-2.71	-4.75	9.36	16.39
	16,000	10.17	17.81	1.63	2.85	-3.10	-5.43	10.67	18.69

Table 5 Damping properties - step bearing set number 1

	Speed RPM	C_{xx}		$C_{xy} = C_{yx}$		C_{yy}	
		lb-s/in	N-s/cm	lb-s/in	N-s/cm	lb-s/in	N-s/cm
Number 1 Bearing	8,000	125	219	-59	-103	443	776
	10,000	124	217	-58	-102	442	774
	12,000	123	215	-57	-100	441	772
	14,000	122	214	-57	-100	441	772
	16,000	122	214	-57	-100	441	772
Number 2 Bearing	8,000	86	151	-47	- 82	291	510
	10,000	85	149	-46	- 81	287	502
	12,000	84	147	-46	- 81	285	499
	14,000	83	145	-45	- 79	284	497
	16,000	83	145	-45	- 79	283	496

Table 6 Comparison of Sommerfeld number, eccentricity ratio and rigid rotor stability parameter for the six bearing sets at 8000 rpm

Bearing Set No.	Type	K´	θ_s	N = 8000 RPM S	ϵ	ω_s
A	Two Axial Groove	1.0	-	5.3, 4.3	.03, .04	2.1, 2.1
1	Step	2.1, 2.4	145°	3.5, 2.7	.29, .29	7.5, 7.0
2	Step	2.8, 2.6	140°	2.7, 2.7	.28, .28	6.6, 6.6
3*	Step	6.6, 8.6*	150°	3.0, 2.7	.21, .16	4.6, 3.6
4*	Step	3.3, 2.1	90°	3.0, 3.0	.22, .21	4.6, 4.8
5*	Step	11.7, 8.3*	140°	3.8, 2.9	.09, .13	3.0, 3.4

* Off optimum

Table 7 Results of theoretical stability analysis - real part of eigenvalue as a function of speed for step bearing number 1

Speed (RPM)	Real Root (sec^{-1})
8,000	-9.18
10,000	-2.15
11,100*	0.00*
12,000	+1.14
14,000	+2.52
16,000	+3.10

* Interpolated instability onset speed

Table 8 Summary of theoretical instability onset speeds for the six bearing designs

Bearing Set No.	Type	K´	θ_s	Instability Onset Speed (RPM)		Percent Error
				Theoretical	Experimental	
A	Two Axial Groove	1.0	-	6,000	6,600	9.1%
1	Step	2.1, 2.4	145°	11,100	>13,800	>19.6%
2	Step	2.8, 2.6	140°	11,500	9,300	-23.7%
3*	Step	6.6, 8.6*	150°	8,850	8,900	0.6%
4*	Step	3.3, 2.1	90°*	8,100	8,600	5.8%
5*	Step	11.7, 8.3*	140°	7,800	7,800	0.0%

* Off optimum

instability onset speed of the three mass rotor by around 109 and 41 percent compared to the two axial groove bearings. Increasing the film thickness ratio from the near optimum cases, decreases the onset speed. Decreasing the step location angle to 90° from the near optimum locations also decreases the onset speed.

The theoretical stability analysis predicts the general trends in the experimental data. All step bearing designs increase the onset speed over the two axial groove bearings. The near-optimum designs have the highest onset speeds and the off-optimum designs the lowest.

Side rail construction is important in designing step bearings for optimum stability. Care should be taken to insure uniform pocket depth.

Acknowledgments

This work was supported at the University of Virginia in part by ERDA Contract No. EF-76-5-01-2479, directed by D. W. Lewis and the Industrial Sponsored Research Program, directed by E. J. Gunter.

References

1 Wilcock, D. F., and Booser, E. R., *Bearing Design and Application*, McGraw-Hill, New York, 1957.

2 Hamrock, B. J., and Anderson, W. J., "Rayleigh Step Journal Bearing, Part II - Incompressible Fluid," ASME, *Journal of Lubrication Technology*, Vol. 90, 1969, pp. 641–650.

3 Putre, H. A., "Computer Solution of Unsteady Navier-Stokes Equations for an Infinite Hydrodynamic Step Bearing," NASA TN D-5682, Lewis Research Center, Cleveland, Ohio, April, 1970.

4 Schuller, F. T., "Experiments on the Stability of Various Water-Lubricated Fixed Geometry Hydrodynamic Journal Bearings at Zero Load," ASME, *Journal of Lubrication Technology*, Oct. 1973, pp. 434–446.

5 Smalley, A. J., Vohr, J. H., Castelli, V., and Wachmann, C., "An Analytical and Experimental Investigation of Turbulent Flow in Bearing Films Including Convective Fluid Inertia Forces," ASME, *Journal of Lubrication Technology*, Vol. 96, No. 1, 1974, pp. 151–157.

6 Allaire, P. E., Nicholas, J. C., and Barrett, L. E., "Analysis of Step Journal Bearings - Infinite Length, Inertia Effects," to be published in ASLE Trans., No. 78-AM-38-1.

7 Nicholas, J. C., and Allaire, P. E., "Analysis of Step Journal Bearings - Finite Length, Stability," to be puslished in ASLE Trans., No. 78-LC-6B-2.

8 Nicholas, J. C., Allaire, P. E., and Lewis, D. W., "Stiffness and Damping Coefficients for Finite Length Step Journal Bearings," to be published in ASLE Trans., No. 79-AM-6D-1.

9 Leader, M. E., Flack, R. D., and Allaire, P. E., "Experimental Study of Three Journal Bearings with a Flexible Rotor," to be published in ASLE Trans. No. 79-AM-6D-2.

10 Flack, R. D., Leader, M. E., and Gunter, E. J., "An Experimental Investigation on the Response of a Flexible Rotor Mounted in Pressure Dam Bearings," submitted to ASME, *Journal of Mechanical Design*.

11 Allaire, P. E., Nicholas, J. C., and Gunter, E. J., "Systems of Finite Elements for Finte Bearings," ASME, *Journal of Lubrication Technology*, Vol. 99, No. 2, Apr. 1977, pp. 187–197.

12 Lund, J. W., "Stability and Damped Critical Speeds of a Flexible Rotor in Fluid-Film Bearings," ASME, *Journal of Engineering for Industry*, Vol. 96, No. 2, May, 1974, pp. 509–517.

Printed in U.S.A.